



Deposition of polymer films by spin casting: A quantitative analysis

José Danglad-Flores^{a,b}, Stephan Eickelmann^b, Hans Riegler^{b,*}

^a Institut für Chemie, Technische Universität Berlin, Strasse des 17. Juni 135, D-10623 Berlin, Germany

^b Max-Planck-Institut für Kolloid- und Grenzflächenforschung, D-14476 Potsdam-Golm, Germany



HIGHLIGHTS

- A consistent and uncomplicated theoretical description for spin coating is reported.
- We show quantitative insight into the processes occurring during the spin cast process.
- We present practical method to predict the final solute coverage based on bulk.
- Solution properties and a single “calibration” experiment.

ARTICLE INFO

Article history:

Received 19 September 2017

Received in revised form 11 December 2017

Accepted 7 January 2018

Available online 8 January 2018

Keywords:

Spin-coating
Spin-casting
Polymer films

ABSTRACT

Spin casting of mixtures of nonvolatile polymeric solutes dissolved in volatile solvents is studied experimentally and theoretically. The final solute coverage, time-resolved film thinning, time-resolved solvent evaporation, and evolution of the solute concentration within the thinning film is investigated for various combinations of different polymers (PMMA, PS, PS-*b*-PMMA) and different solvents (toluene, ethylacetate) for a wide range of polymer concentrations and spin cast conditions. The comprehensive data unveil a clear picture of the spin cast process. The findings are translated into a concise theoretical description. Easily available bulk properties of the solvent/solute mixture plus a single “calibration” experiment are sufficient for a quantitative description of the spin cast process including a prediction of the final solute coverage. This and the well-specified boundary conditions render the approach useful for practical applications.

© 2018 The Authors. Published by Elsevier Ltd. This is an open access article under the CC BY license (<http://creativecommons.org/licenses/by/4.0/>).

1. Introduction

Spin casting (spin coating) is a widely used technique to deposit films of uniform thickness on planar solid substrates (Frank et al., 1996; Larson and Reh, 1997; Norrman et al., 2005). In this process a liquid melt or solution is deposited on a rotating substrate. During a transient period the combination of radial and hydrodynamic (viscous) forces will flatten the deposited liquid bulk into a planar film. With on-going rotation this planar film will continuously become thinner (Emslie et al., 1958; Acrivos et al., 1960). If the liquid film consists of a nonvolatile solute and a volatile solvent, film thinning also occurs due to solvent evaporation in addition to the hydrodynamic thinning. In the beginning, with thicker films, film thinning will be dominated by hydrodynamics. With thin films evaporation will dominate the film thinning process. Hence, to a first approximation spin casting of volatile liquids can be considered as a sequence of hydrodynamic planar film formation and thinning followed by evaporative thinning/drying of this film

(Meyerhofer, 1978). If the liquid consists of a mixture of a non-volatile solute and a volatile solvent, the solvent evaporation causes a continuous enrichment of the nonvolatile solution components. In the end, the solute will be deposited as a dry film.

Even assuming idealized hydrodynamic and evaporative behavior, film thinning and the accompanying solute enrichment is a rather complicated process, because the increasing solute concentration has an influence on the hydrodynamic and on the evaporative properties of the film. Viscosity and evaporation behavior change continuously during film thinning. In addition, because the evaporation occurs from the film surface, the vertical solute concentration profile within the thinning film changes with time, possibly leading to a high solute enrichment close to the surface (“skin formation” (Haas et al., 2000), “crust” effect (De Gennes, 2002)). The combined process of hydrodynamic and evaporative film thinning has been investigated in quite a number of theoretical and experimental studies (Meyerhofer, 1978; Shimoji, 1987; Bornside et al., 1989; Jenekhe, 1984; Lawrence, 1988; Flackr and Soong, 1984; Ohara et al., 1989; Lawrence, 1990; Reisfeld et al., 1991a,b; Shimoji, 1989; Sukanek, 1991).

* Corresponding author.

E-mail address: hans.riegler@mpikg.mpg.de (H. Riegler).

A practically useful theoretical analysis of the hydrodynamic-evaporative spin cast process should describe quantitatively how under the given (initial) process parameters (rotation, evaporation rate, liquid viscosity, etc.) the film thickness and its composition evolves with time. In particular, it should predict the final solute coverage. This has been done recently (Karpitschka et al., 2015) in a “zero-order” approach. For this approach it was assumed that the viscosity and the evaporation rate of the solution remains constant throughout the entire process of hydrodynamic-evaporative thinning. The values of viscosity and evaporation rate are assumed identical to those of the pure solvent. Based on easily measurable quantities this rather simple approach predicts the final solute film thickness (solute coverage) with remarkable quantitative precision for low solute concentrations (i.e., for final solute film thicknesses of up to several tens of nanometers). In the following we investigate at which solute concentrations this “zero-order” approach starts to fail quantitatively and how it can be extended in a simple and practically feasible way into a “first-order” approach for higher solute concentrations i.e., higher final film thickness.

To this end we measure and analyze in detail the hydrodynamic-evaporative thinning of solution films and the final solute coverages as a function of the solute concentrations for various solutes and solvents. This reveals at which solute concentrations the thinning behavior and final coverage starts to deviate significantly from the “zero-order” approach. Based on these results we present a “first-order” description of the spin cast process. The findings offer a rather simple and practically applicable recipe to quantitatively predict final solute film thickness of up to micrometers.

1.1. Zero-order scenario for hydrodynamic-evaporative film thinning

The thinning of a Newtonian, volatile liquid film of thickness h on a rotating support is described by Meyerhofer (1978):

$$dh/dt = -2Kh^3 - E. \quad (1)$$

Eq. (1) assumes no slip at the liquid/substrate interface (lubrication approximation) and a free liquid surface. The film thinning due to contribution from surface tension and gravity is neglected (Emslie et al., 1958; Meyerhofer, 1978; Karpitschka et al., 2015). E is the evaporation rate. The parameter

$$K = \omega^2/(3\nu). \quad (2)$$

describes the hydrodynamic behavior (ω = rotational speed, ν = kinematic viscosity). The parameters characterizing the process according to Eq. (1) are K and E . In the zero-order approximation (Karpitschka et al., 2015) they determine t_{sc} , the total spin cast time (film thinning from $h \rightarrow \infty$ to $h = 0$):

$$t_{sc} = (2\pi/3^{3/2})(2E^2K)^{-1/3}. \quad (3)$$

E and K also determine the “transition height” h_{tr} , which identifies the film thickness of the transition from film thinning dominated by hydrodynamics to thinning dominated by evaporation:

$$h_{tr} = (E/2K)^{1/3}. \quad (4)$$

Because at thicknesses of less than h_{tr} film thinning is mostly due to evaporation, most of the solute, which is contained in the film of thickness h_{tr} (with a solute concentration approximately equal to the weighing in concentration x_0), is finally deposited on the substrate. This leads to the final film thickness of the solute¹:

¹ The change in the total volume from the h_{tr} to the dry film is proportional to the solute volume fraction; because the area is constant this proportionality can be translated to the film height; it is practical in most of the cases assume that the volume fraction is equal to the mass fraction (x_0) when solution and solute density are approximately the same $\rho_L \approx \rho_S$.

$$h_f = x_0 \frac{\rho_L}{\rho_S} h_{tr} = x_0 \left(\frac{3Ev}{2\omega^2} \right)^{1/3} \approx 0.8x_0 (K/E)^{-1/3}. \quad (5)$$

where are the shortcomings of the zero-order approach? For Eqs. (4) and (5) it is assumed that K and E are constant up to a film thickness of h_{tr} . For Eq. (3) it is assumed that K and E are constant during the whole spin cast process. These assumptions are never perfectly correct, because K and E depend on the solute concentration x (which increases continuously due to the solvent evaporation). But for small initial x_0 the absolute increase of solute during film thinning is small even for films much thinner than h_{tr} . Thus Eqs. (4) and (5) are pretty accurate and even Eq. (3) is quite exact.

In the following we will explore what means “small” initial x_0 with respect to Eqs. (3)–(5) i.e., for which x_0 and at which film thicknesses do film thinning behavior $h(t)$ and final thickness h_f significantly deviate from the “zero-order” scenario (Karpitschka et al., 2015). We will also explore the reason of the deviation from the “zero-order” scenario and show how it can be modified in a most simple and practical way, so that quantitative predictions on h_f , on the film thinning behavior $h(t)$, and on the behavior of the solute concentration can be made with a minimum of practical effort based on easily measurable system parameters.

It should be noted that for the zero-order analysis as well as for the first-order approach discussed in the following it is assumed that during the spin cast process the deposited liquid forms a film of uniform thickness, whose thinning is dominated by hydrodynamic flattening in the beginning of the process. The analysis will not be applicable if evaporation changes the solution composition markedly already during the initial transient process when the solution is deposited on the rotating substrate, flattening and forming a planar film. In view of the properties of the solution this means that evaporation rate and viscosity have to be sufficiently low. In view of the spin cast process this means that the deposited amount of liquid has to be sufficiently large, because the evaporative losses of the initially deposited liquid drop scale approximately with its linear dimension i.e., with radius r (Picknett and Bexon, 1977; Birdi et al., 1989; Soulie et al., 2015), whereas the time for the liquid flattening scales approximately with the inverse of the linear dimension i.e., with $1/r^2$ (see Emslie et al. (1958)). It turns out that typical liquids applied in spin casting, such as toluene or water, deposited in typical quantities (drops of 100 μ l and more) on samples of typically a few cm^2 easily meet these conditions as can easily be estimated.²

2. Materials and methods

2.1. Chemicals

Block copolymers of polystyrene and polymethylmethacrylate (PS-*b*-PMMA) Mn $\times 10^3 = 55$ -*b*-22; $\rho = 945 \text{ kg/m}^3$ (“A”); polystyrene (“PS”) Mn $\times 10^3 = 25$ (“B”), 50 (“C”) and 195 (“D”); polymethylmethacrylate (“PMMA”) Mn $\times 10^3 = 996$ (“E”) were

² A rather crude estimation (derived from Fig. 2 of the paper of Emslie et al. (1958)) shows that 200 μ l of toluene deposited as a sessile drop with a Gaussian contour on a substrate rotating at 1000 rpm (i.e., $K \approx 6 \times 10^9 \text{ s/m}^2$) will theoretically become a flat pancake of uniform thickness within $t = 1/(Kr^2) \approx 10 \mu\text{s}$. On a planar substrate of about 1 cm^2 area this planar film is about 100 μm thick. The evaporation rate of toluene for a planar film rotating at 1000 rpm is about 1 $\mu\text{m/s}$. In this case the evaporative losses within the flattening time of 10 μs will lead to a loss of about 1 nm toluene film, which will reduce the film thickness by a factor of only 10^{-5} (=1 nm/100 μm). In reality the time from a round drop touching the rotating substrate to a planar film through a sessile drop will last longer than only 10 μs . But by and large this crude estimation shows that for the given conditions (toluene, drop volume, sample size) evaporation can be neglected during the initial flattening process and the zero-order approximation of the spin cast process can be applied (which is confirmed by experiments (Karpitschka et al., 2015)).

obtained from Polymer Source Inc. Toluene (“TO”, 99.9%; $\rho = 856 \text{ kg/m}^3$) was from Sigma Aldrich, ethylacetate (“EA”, 99.5%; $\rho = 900 \text{ kg/m}^3$) from Chemsolute.

The viscosity of PS(55.000)-b-PMMA(22.000) dissolved in toluene at concentrations from 0.001 to 0.15 w/w was measured with a Shear Rheometer Anton Paar MCR 301 in the cone-plate mode rotating between 1000 and 3000 rpm at 25 °C.

2.2. Substrates

As substrates served silicon wafer pieces of $\approx 2 \times 2 \text{ cm}^2$ with natural oxide surfaces (oxide layer thickness $\approx 2 \text{ nm}$) or with artificial oxide layers of $(50 \pm 1) \text{ nm}$ thickness. In both cases the surface roughness was $\approx 0.5 \text{ nm}$.

2.3. Substrate surface preparation

The substrates were first cleaned in an ultrasonic bath by a sequence of immersions (for 10 min each) in: (1.) deionized water, (2.) ethanol, (3.) acetone, (4.) ethanol, and (5.) deionized water. In a second cleaning step they were immersed in piranha solution ($\text{H}_2\text{O}_2(35\%)/\text{H}_2\text{O}(65\%)$ and 96% H_2SO_4 , 1:3 volume ratio) for 30 min. Finally they were again immersed and sonicated for 10 min in deionized H_2O and stored therein. Just before use they were dried by blowing with dry N_2 (purity: 5.0).

2.4. Spin casting

0.2 mL of solution were deposited on the center of the substrate (already rotating at constant speed). After polymer deposition, the wafers were dry blown with N_2 and then stored for 1 day before the coverage (film thickness) was determined by ellipsometry.

2.5. Optical imaging

For the in situ observation of the spin coating process, a modified optical microscope (Axio Scope A1 from Zeiss) was used. The light source was a blue diode laser (6 W, 445 nm, LDM-445-6000, LASERTACK, de-speckled by a combination of liquid light guide and a rotational diffusor). The spin coater is mounted on a X-Y table. Microscopy was performed from the top in interference enhanced reflection mode (Köhler et al., 2006). A high speed monochromatic camera (1000 fps) and suitable image triggering and processing provided single frames during the film thinning (Manske et al., 1990). Interferometric data (brightness variations during film thinning) revealed the film thinning behaviour (Peurrung and Graves, 1991).

2.6. Measurement of the final coverage

The thicknesses, h_f , of the dry polymer films (equivalent: coverages Γ) were determined by ellipsometry for thickness up to 150 nm; above 150 nm it was determined by measuring the depth of a scratch by AFM. The index of refraction of the uncoated silicon substrate was measured as 3.86 (silicon), the one of the silica layer as 1.46. The index of refraction of PMMA was assumed as 1.49 (Baker and Dyer, 1993). The index of refraction of PS was assumed 1.58 (Ay et al., 2004) and 1.56 for the block copolymer. These indices were derived from comparisons of the film thicknesses respectively coverages measured by AFM and ellipsometry in the range between 20 and 100 nm.

3. Results

Fig. 1 depicts the thicknesses h_f of block copolymer (PS-PMMA) films deposited from polymer/solvent solutions with various different initial (weighing in) polymer concentrations x_0 and different solvents (TO and EA). For low concentrations up to about $x_0 \approx 0.02$ film thicknesses h and the initial polymer concentrations x_0 are linearly proportional in agreement with Eq. (5) (top panel (A)). For higher polymer concentrations the film thickness is much higher than predicted (for $x_0 = 0.15$ by more than a factor of 3) as depicted in the lower panel (B). The dashed line in panel (B) shows the predicted coverage according to Eq. (5) of the “zero order” approximation. Measurements with other solute/solvent combinations yield similar results (see below).

Fig. 2 shows the experimentally measured thinning curves for pure toluene and various solutions of PS-b-PMMA in toluene including a measurement with a rather high polymer concentration of 0.15 (w/w) depicted separately in the inset. The thinning curves presented in this figure originate from the same experiments that lead to the film thicknesses depicted in Fig. 1. The different curves are plotted with different offsets in time (shifted laterally) to enable their presentation within the same figure without overlapping. The solid (fitting) lines are the theoretically predicted thinning curves based on the first-order spin cast scenario presented below. In all cases the thinning occurs in the beginning rather rapidly, slows down, proceeds then linearly for some time until it slows down rather rapidly to end upon reaching the final height of the deposited polymer layer. For the lowest polymer concentrations the final thickness of the deposited film is barely visible with the scaling applied in Fig. 2. With the weighing in polymer concentrations exceeding about 1% the finally deposited polymer film clearly shows up in the curves. For $x_0 = 0.15$ initial polymer concentration the deposited polymer film is about 2.5 μm thick (see inset).

For polymer concentrations of up to about $x_0 = 0.02$ the cross-over between the regime of steep and nonlinear hydrodynamic thinning and the linear regime of evaporative film thinning is clearly discernible. This transition range reveals h_{tr} (the h_{tr} indicated in the figure is the result of a fit of the thinning curve based on the first-order spin cast theory as presented below). With pure toluene h_{tr} is about 5.2 μm . The transition height increases with increasing polymer concentration. With sufficient precision h_{tr} can be derived quantitatively from fitting the experimentally measured thinning curves only for small x_0 . With larger x_0 the cross-over between hydrodynamic and evaporative thinning is getting too close to the early transient film formation process when the liquid undergoes the transition from a drop to a film. Therefore, in this case h_{tr} cannot be derived with reasonable accuracy from the experimentally measured thinning curves. On the other hand, all thinning curves presented in Fig. 2 display a rather wide range of a rather linear thickness decrease before the film thinning decreases rapidly due to the final polymer deposition/drying process. Presumably this linear range reflects film thinning dominated by evaporation.

Fig. 3 presents the slopes, $|dh/dt|$, of the experimentally measured film thinning curves (Fig. 2) as a function of the time and the polymer concentrations. The indicated polymer concentrations, x_0 , are the original weighing in values. The time is scaled with the process time, t_{sc} (which is derived/defined with the first-order approach as discussed below). Scaling the time with t_{sc} allows for a convenient presentation of all data in a single plot without too much stretching of the time axis (with increasing x_0 film thinning takes increasingly longer, as demonstrated in particular by the data presented in the inset of Fig. 2). Fig. 3 reveals for all thinning curves a regime of film thinning with a constant slope, intermediate

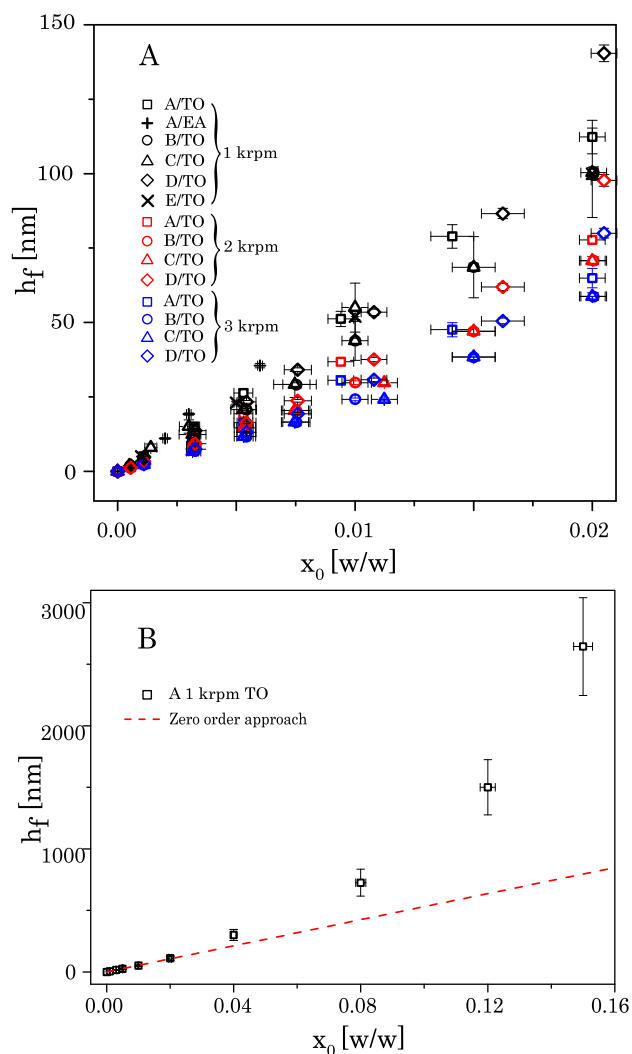


Fig. 1. Final film thicknesses h_f measured by ellipsometry and AFM for (A) PS-*b*-PMMA ($M_n \times 10^3 = 55$ -*b*-22); (B) PS ($M_n \times 10^3 = 25$); (C) PS ($M_n \times 10^3 = 50$); (D) PS ($M_n \times 10^3 = 95$); (E) PMMA ($M_n \times 10^3 = 996$) deposited from solutions in toluene (TO) and ethylacetate (EA) with various concentrations x_0 . The sample rotations are denoted in krpm = 1000 rpm. The top panel (A) shows that for low polymer concentrations up to $x_0 \approx 0.02$ film thickness and x_0 are linearly proportional in agreement with the “zero-order” model (Eq. (5)). For $x_0 > 0.02$ (i.e., $h > 50$ nm) (panel (B)) h_f is increasingly much thicker than predicted in the zero-order calculation.

between the early nonlinear hydrodynamic film thinning and the nonlinear drying behaviour at the end of the spin cast process. Except for the experiments with the highest initial polymer concentration ($x_0 = 0.15$), the range of constant slope as well as the slopes therein are nearly identical for all polymer concentrations. For $x_0 = 0.15$ the range of constant slope is shifted to relatively earlier times, but the slope therein is still quite similar to the cases of lower polymer concentration. According to the film thinning scenario (Eq. (1)) this (constant) slope identifies the evaporation rate E of the liquid film after the film thinning ceases to be dominated by hydrodynamic forces.

At the end of a range with approximately constant slope $|dh/dt|$ (i.e., constant E), $|dh/dt|$ abruptly decreases. This sudden decrease of E is quite pronounced for the higher polymer concentrations. For low x_0 the sudden decrease occurs at rather thin films and only within a rather short time. Supposedly this late and rather slowly proceeding film thinning after the range with $|dh/dt|$ can be attributed to the final drying of a thin, polymer-rich film.

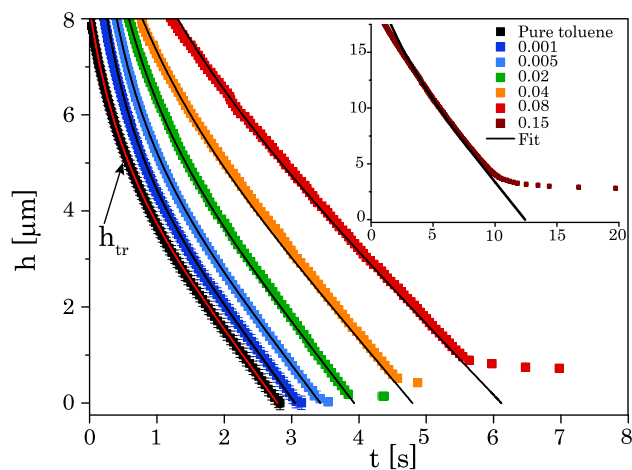


Fig. 2. Experimentally measured thinning curves of pure toluene and various solutions of PS-*b*-PMMA (MW:55k-*b*-22k) in toluene at 1000 rpm. For better visualization the curves are shifted laterally to each other on the time axis. Indicated for the pure toluene is also the transition height as they can be derived from fitting the thinning curve. The solid lines are the theoretical thinning curves according to the first-order model (see main text).

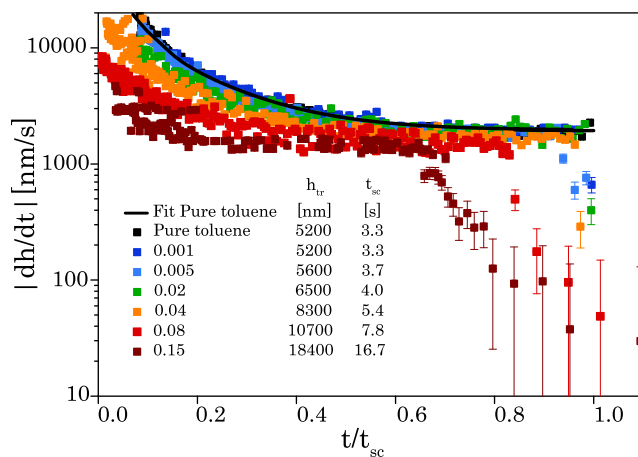


Fig. 3. Slopes of the thinning curves as function of the time. The time is rescaled by the total process time t_{sc} . The polymer concentrations, x_0 , are the initial weighing in values. The solvent is toluene, the polymer is PS-*b*-PMMA (MW:55k-*b*-22k).

Fig. 4 depicts the experimentally derived evaporation rates, E , as function of the actual polymer concentration x (for PS-*b*-PMMA, MW = 55 k-*b*-22 k, dissolved in toluene). The data are extracted from the results depicted in Fig. 3. To this end it is assumed that film thinning at thicknesses below h_{tr} is dominated by evaporation and accordingly the polymer concentration is given by:

$$x(h) = \frac{h_{tr}}{h} x_0. \quad (6)$$

Fig. 4 reveals that up to a polymer concentration of about $x = 0.05$ the evaporation rate remains identical to the one of pure toluene. Furthermore, even up to about $x = 0.5$ the evaporation rate decreases only by about 25%.

Fig. 5 presents the spin cast parameters, K , as function of x_0 . The inset presents the bulk viscosities of the polymer solutions as function of x_0 measured by a rheometer. The “Experimental K ” values are calculated from the experimentally measured viscosities via Eq. (2). The “Fitted K ” values are derived from best fits of the experimentally measured thinning curves assuming that they are following Eq. (1). For the fits/simulations it is assumed that the evaporation rate is constant and identical to the value revealed by the intermediate, constant slope of the corresponding thinning

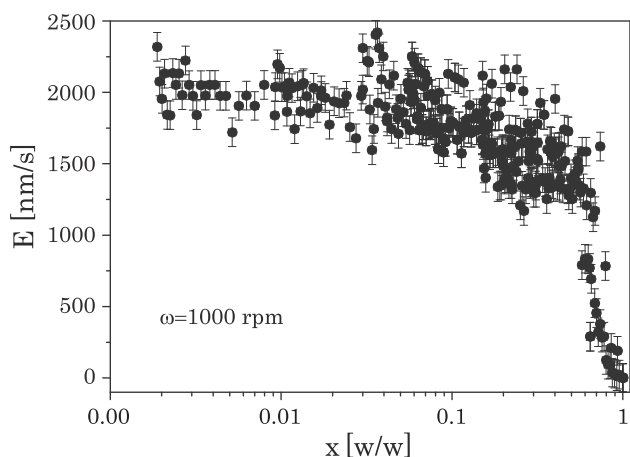


Fig. 4. Evaporation rates E derived from the slopes $|dh/dt|$ of the experimentally measured thinning curves of film thicknesses below h_{tr} as function of the polymer concentration. Because $h < h_{tr}$ evaporative thinning dominates and $dh/dt = E \cdot x$ is the polymer concentration within the film corresponding to the measured E . It is derived from the original weighing in value, x_0 , by taking into account the loss of solvent due to evaporation. The data were recorded at $\omega = 1000$ rpm.

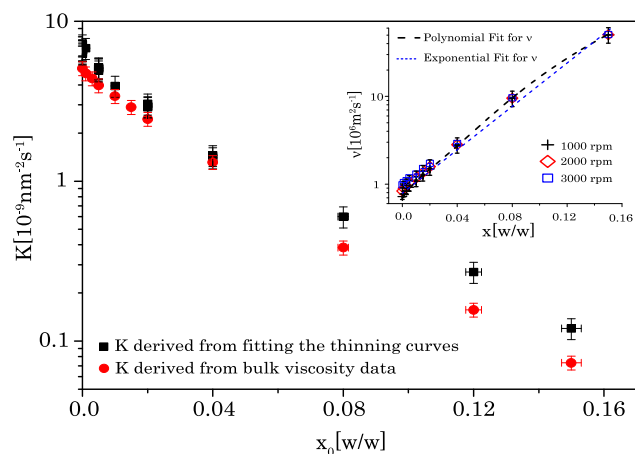


Fig. 5. Spin cast parameters K plotted as a function of x_0 , the weighing in polymer concentration (MW:55k-b-22k, dissolved in toluene). The full black squares present K derived from best fits of the experimentally measured thinning curves according to Eq. (1) and assuming (constant) evaporation rates E as derived from the intermediate, constant slope of the thinning curve (For the fits the thinning behavior (Fig. 4) during the initial transient transformation from a drop to a film of uniform thickness as well as the thinning during the final film drying is neglected). The full red circles in the main frame depict K calculated with Eq. (2) from the viscosities obtained by the bulk measurements (see inset). The inset shows the dynamic bulk viscosities from bulk solutions at different concentrations and shear speeds (measured with a rheometer Anton Paar MCR 301). Also shown are fits of the bulk viscosity data (dashed: polynomial; dotted: exponential; see also main text). (For interpretation of the references to colour in this figure legend, the reader is referred to the web version of this article.)

curve as depicted in Fig. 4 (i.e., essentially assuming in all cases the same E of $\approx 1.8 \mu\text{m/s}$ except for $x_0 = 0.15$ with $E = 1.5 \mu\text{m/s}$). Fig. 2 shows some examples of such fits together with the corresponding experimental data.³

³ The fits assume that the thinning curves start at infinite thickness and end at zero thickness without any polymer/solute deposition i.e., a pure solvent with the E and K of the real polymer solution. It therefore focuses only on the experimental data in the range (1) after the transient film formation at the beginning of the spin cast process and (2) before the thinning curve shows the deposition of a polymer film at the end of the process. The deviations of the real thinning curve from an idealized thinning curve at the beginning and at the end of the real spin cast process are quite obvious so that the upper and lower cutoff for the fitting range is quite unambiguous.

The inset of Fig. 5 shows that the viscosities of the polymer solution changes by about 2 orders of magnitude if the polymer concentration increases from $x = 0$ to $x = 0.15$. The solutions were investigated at three different speeds. As can be seen they behave like a Newtonian fluid. The experimental data could be fitted quite nicely with a polynomial of third order ($v = 10^6 \rho^{-1} (13.3x^3 - 0.29x^2 + 0.035x + 0.0006)$) following Ref. (Mate and Novotny, 1991) as well as exponentially ($v = 700 \rho^{-1} \exp(28.5x)$) according to Refs. Borside et al. (1991) and Phillis (1995); the density of the solution was taken as mass fraction proportionality from the density of each component (see Materials and methods).

The change of two orders of magnitude in v is reflected in the decrease of K , which decreases by nearly two orders of magnitude when the polymer concentration increases from $x_0 = 0$ to $x_0 = 0.15$. Fig. 5 reveals that K derived from fitting the thinning curves and K derived from bulk viscosity data agree quite well within the entire range of polymer concentrations. This means that the experimentally measured thinning curves up to $x_0 = 0.1$ can be described by Eq. 1 with a constant E identical to the one of the pure solvent and K values based on the viscosity of the bulk solutions with the weighing polymer concentrations x_0 .

Fig. 6 supports this assumption by presenting the time evolution of the polymer concentration x as derived according to Eq. (6) as a function of time. The time is scaled with an empirical process time t_{sc}^* , which is a combination of the t_{sc} plus the additional time for complete solute drying (i.e., when $dh/dt = 0$) as derived from the empirical thinning curves. The black solid lines are derived from fits to the experimentally observed thinning behavior assuming the thinning behavior according to Eq. (1) with a constant E (of the pure solvent) and constant K based on the bulk viscosities of the initial solution as shown in Fig. 5. The experimental data agree with the theoretical curves up to concentrations of about $x \approx 0.65$ or even higher (for the lower initial x_0). At concentrations higher than $x \approx 0.65$ the polymer enrichment slows down (as can also be seen in Fig. 4).

Fig. 7 presents the evaporation rates as function of the square root of the sample angular speed, $\omega^{1/2}$ (Cochran, 1934; Meyerhofer, 1978; Haas et al., 2000). For $\omega = 0$ the evaporation rates were derived from the loss of weight per time for a petri dish (5 cm diameter, about 0.5 cm deep) filled with solutions in a non-convective ambient air environment.⁴ The evaporation rates for the range of $500 \text{ rpm} < \omega < 4000 \text{ rpm}$ were derived from the linear sections of the thinning curves. Fig. 7 shows that the data can empirically be described by:

$$E(\omega) = e_0 + e\sqrt{\omega}, \quad (7)$$

An excellent approximation for Eq. (7) for the case of spin casting (i.e. $\omega > 1 \text{ rps}$) is:

$$E(\omega) \approx e\sqrt{\omega} \quad (8)$$

Fig. 8 presents the experimentally measured final polymer film thicknesses, h_f , as function of the initial weighing in polymer concentrations x_0 . The final film thicknesses are scaled by the transition heights, h_{tr} , of the corresponding systems. The data are from different polymers, different solvents, and different speeds of rotation. They agree very well with a linear behavior between the final

⁴ Surface curvature, convection and side walls influence the static evaporation rate and have to be minimized for its experimental determination. Petri dishes with several centimeters in diameter filled to the rim and placed in the nearly completely closed compartment of a precision scale are a reasonably optimized compromise of an experimental setup. Convection is suppressed, the surface is mostly planar, the liquid volume is relatively small and the loss of weight can be measured with high sensitivity/precision.

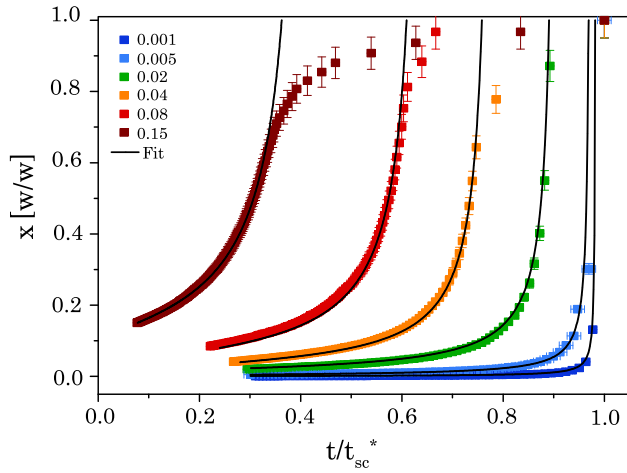


Fig. 6. Time evolution of the polymer concentration x during film thinning for different initial x_0 . The time is scaled with an empirical process time t_{sc}^* ($t_{sc}^* = t_{sc} + a$ with $a =$ an additional time taking into account complete solute drying as derived from the empirical thinning curves (i.e., when $dh/dt = 0$). The concentration evolution is derived from the empirical thinning curves with $x = x_0 * h_{tr}/h$. The black solid lines are derived from fits to the experimentally observed thinning curves assuming ideal thinning behavior according to Eq. (1) with a fixed E of the pure solvent and a fixed K based on the bulk viscosities of the initial solution as shown in Fig. 8.

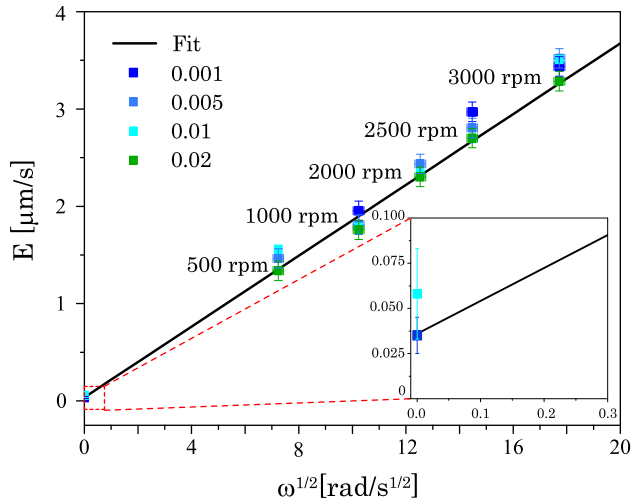


Fig. 7. Experimentally measured evaporation rates, E , for various polymer concentrations x_0 as function of the sample rotation rates ω (PS-PMMA, MW:55k-b-22k, dissolved in toluene). The inset shows the static evaporation rate ($\omega = 0$) as measured from the evaporative weight loss of the solution in a petri dish in still air.

film thickness of the deposited non-volatile solute, h_f , and the initial (weighing in) concentration, x_0 , of the solute according to Eq. (5), where $E (=E(\omega))$ has been replaced by e according to Eq. (7):

$$h_f = x_0 \left(\frac{3e v_0}{2\omega^{3/2}} \right)^{1/3} = x_0 \left(\frac{3e \eta_0}{2\rho_0} \right)^{1/3} \omega^{-1/2}. \quad (9)$$

or, assuming that the (weighing in) density of the solution, ρ_0 is independent for the polymer concentration:

$$h_f = c * x_0 \left(\frac{\eta_0}{\rho_0} \right)^{1/3} \omega^{-1/2}, \quad (10)$$

with

$$c = \left(\frac{3e}{2} \right)^{1/3}, \quad (11)$$

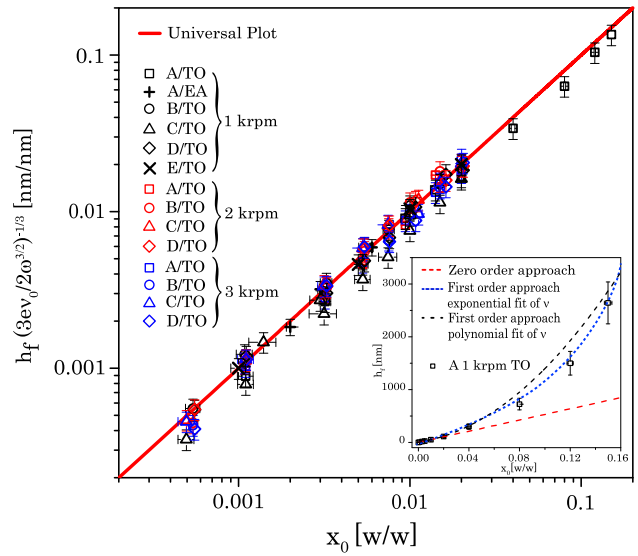


Fig. 8. Final film thicknesses, h_f , as function of the initial weighing in polymer concentrations x_0 . Data are shown for various combinations of polymers, solvents and rotational speeds. h_f is scaled by $\left(\frac{3e v_0}{2\omega^{3/2}} \right)^{1/3}$ assuming constant evaporation rates e of the corresponding solvent (180 nm/s^{1/2} for TO and 610 nm/s^{1/2} for EA) and the bulk kinematic viscosities v_0 of the solutions with concentration x_0 . The inset shows h_f for polymer A dissolved in TO as function of the initial weighing in polymer concentration x_0 . The dotted line shows h_f predicted according to the zero order approach (see Fig. 1). The solid line shows h_f according to the first order approach resulting from Eq. (9) with constant e and bulk viscosity properties v_0 . The red dashed line shows h_f predicted according to the zero order approach (see also Fig. 1). The black dashed line shows h_f according to the first order approach from Eq. (9) with constant e and bulk viscosity properties v_0 as presented in Fig. 5 and fitted by an exponential rheological behaviour. The blue dotted line shows the polynomial fit of the bulk rheological behaviour.

as an instrument and solvent-specific constant, c , reflecting the evaporative conditions of the used solvent in the applied spin cast setup.⁵ We developed Eqs. (9)–(11) to predict the final solute film thickness, h_f , as a function of the four main process parameters, $x_0, \omega, \eta_0/\rho_0$ and e for a given instrument. All parameters (instrument- or process-specific) are easily measurable. They are either (1) weighing-in properties (η_0, ρ_0), easily accessible by bulk measurements, (2) at hand, adjustable process parameters (x_0, ω), or (3) parameters accessible with one single experiment (e from the measurement of h_f for a given set of η_0, ρ_0, x_0 , and ω).

4. Discussion and conclusion

In this report we analyze the deposition of polymer films onto planar substrates by spin casting polymer solutions with volatile solvents. Our focus is on measuring and understanding in detail how the hydrodynamically flattened solution film gets thinner due to hydrodynamics and evaporation, and finally forms a dry polymer film. We are interested in particular on the behavior of solutions with a relatively high polymer concentration, which lead to final dry polymer film thicknesses of up to several micrometers. In this case the simple zero-order approach that was presented earlier (Karpitschka et al., 2015), which essentially neglects the impact of the dissolved solute on the spin cast process, is quantitatively not correct any more. Fig. 1 reveals experimentally above which weighing in solute concentrations, x_0 , the zero order approach fails quantitatively with respect of the predicted final

⁵ the evaporative conditions are quite similar for different spin cast instruments, as long as the ambient vapor phase is not coming close to becoming saturated with the solvent vapor. The main parameter affecting the evaporation is the rotation.

film thickness. Details on the film thinning behavior for different polymer concentrations are presented in Fig. 2. Its analysis (Fig. 3) reveals the “real” evaporation rates during film thinning (Fig. 4) i.e., the evaporation rates for films of an actual polymer concentration x that results from the polymer enrichment due to the solvent evaporation. It is found that the evaporation rates are barely affected by the polymer concentration up to $x \approx 0.5$. This can be understood because (1.) of the relatively low molar solute concentration even for large x and (2.) there is barely any relative enrichment of polymer close to the film surface. The solute enrichment close to the surface can be estimated as follows: The vertical solute distribution is determined by the competition between the solute enrichment close to the film/air interface due to the solvent evaporation and the solute dilution due to diffusion away from the film/air interface. The relative strength of these antagonistic effects is characterized by the Sherwood number (Karpitschka et al., 2015) (Peclet number, mass transfer Nusselt number). With diffusion coefficients D of typically $\geq 10^{-11}$ m²/s for the polymers used, $Sh_{h_{tr}}$, the Sherwood number at h_{tr} , is smaller than 1. This small Sherwood number means that the vertical solute distribution within the thinning film is rather uniform at h_{tr} . It also means, to a first approximation, that the solute composition is even more uniform as the film is getting thinner than h_{tr} due to evaporation⁶.

The data of Fig. 3 show that the evaporation rates are essentially those of the pure solvent for up to $x \approx 0.5$. E decreases only significantly for $x > 0.5$, indicating a drying process of the polymer-rich solution at these polymer concentrations (Guerrier et al., 1998). Still, even with $x > 0.5$ a pronounced polymer enrichment at the film surface (“crust” or “skin” formation) is not likely, because in this case the evaporation rate would decrease much steeper than observed (Okazaki et al., 1974). Due to the rather constant evaporation rates (Fig. 4) for films much thinner than h_{tr} even for $x > 0.02$, E can be excluded as main reason for the deviation between the measured final film thicknesses and the ones predicted by the zero order analysis. Instead, as main cause for this discrepancy we identify the substantial increase in viscosity with increasing polymer concentration as depicted in Fig. 5. Most remarkable, K_0 i.e., the weighing in kinematic viscosity ν_0 is the key parameter, which determines the final film thickness h_f . Its impact on the final film thickness results from its impact on the transition height, h_{tr} . With decreasing K the transition between hydrodynamic and evaporative thinning is shifted to larger film thicknesses, resulting in thicker final solute film thicknesses, h_f . The variation of K respectively ν during film thinning has no influence on h_f , because this variation occurs essentially during evaporative film thinning. In this case the amount of solute per film area i.e., h_f , remains constant. Fig. 7 presents experimental data on the evaporation rates as function of the rotation speed including the case of $\omega = 0$. The findings confirm the square root dependency that has been discussed already in the literature (Meyerhofer, 1978; Haas et al., 2000; Cochran, 1934).

Fig. 8 presents in a universal plot the relation between the final thicknesses, h_f , and the initial polymer concentration, x_0 , for different polymers, solvents and rotation speeds. The final film thickness is normalized with the transition heights of each experiment based on solvent-specific and instrument-specific evaporation rates e , as well as ν_0 , the measured weighing in kinematic viscosity of the solutions. The excellent agreement between the measured data and the data calculated with Eq. (10) demonstrates the validity of the first-order approach leading to Eq. (10). It is an astonishingly simple correction to the zero-order approach. One has just to

replace the viscosity of the pure solvent by the viscosity of the solution. Eq. (10) is very useful for practical spin cast applications because η_0 and ρ_0 are easily measurable bulk properties. Also accessible right away is ω . And the solvent- and instrument-specific value for e can be determined with just one experimental measurement of h_f through Eq. (10).

We are fully aware that there can be found in the literature quite a number of experimental and theoretical studies addressing similar topics as analyzed in this report (Larson and Rehg, 1997).

However, what has been published before is often patchwork, presenting bits and pieces of different aspects of spin casting. The experimental findings are often confusing, presenting a plethora of data without clear dependencies on parameters and without well-defined boundary conditions.

In particular the relation between the final solute film thickness and whatever is considered as relevant spin cast parameters is addressed in several previous publications. Indeed data similar to Fig. 1 can be found in the literature (Meyerhofer, 1978; Washo, 1977; Hernandez et al., 2010). On-line thinning curves similar to those of Fig. 2 have also been published before (Weill and Dechenaux, 1988; Heriot and Jones, 2005; Jukes et al., 2005; Mokarian-Tabari et al., 2010; Ebbens et al., 2011; Toolan et al., 2013). However, these data were never analyzed in detail theoretically in respect to a simple, transparent spin cast scenario without a guesswork of adjustable parameters. For instance, experimental findings have been explained with evaporation rates and/or viscosities, which (supposedly) continuously vary during the spin cast process due to the solute enrichment. Thus, based on suitably selected adjustable parameters these models explain the experimental findings. But these earlier models fail to predict the result of a spin cast process quantitatively, in particular on a more general, universal scope, because the models are based only partially on solid experimental data. Up to now nobody has actually measured *in vivo* the evaporation rates during the film thinning and solute enrichment. Data as presented in Figs. 3, 4 and 6 are not available in the literature. The result of these new experimental insights is a rather universal, concise theory, which (1.) accurately predicts the final film thickness for a wide range of thicknesses (Fig. 8), (2.) is based on only a few measurable (bulk) quantities (Eq. (10)), (3.) is supported by experimental data (in particular Fig. 3) and, (4.) is based on a simple, transparent physics approach.

In conclusion, we present here for those who want to apply evaporative spin casting (a solution of a nonvolatile solute and a volatile solvent) a lucid and well-defined “recipe” to achieve a specific solute coverage. In particular, based on detailed experimental investigations, we reveal and discuss in a transparent approach how we extract our final “master” formula (Eq. (10)). Step-by-step we explicitly relate the theoretical description to the experimental observations and specify the boundary conditions of its validity. It turns out that the spin cast process is rather straightforward even for relatively high solute concentrations. Only a few easily measurable bulk system parameters (η_0, ρ_0, ω) and one “calibration” experiment (determination of “ e ”) are sufficient to describe the process and to predict its main result, the final solute coverage. Beyond that, the data and analysis presented in this report disclose a transparent picture on the physics occurring during evaporative spin casting, such as the thinning behavior, the evaporation behavior, and the evolution of the solute concentration.

Acknowledgements

Thanks to Reinhard Lipowsky for institutional support. JDF was funded by the DAAD and DFG through the IRTG 1524. JDF thanks for his training the GISDE, Universidad de Oriente, Venezuela.

⁶ $Sh = (Eh)/D$ with E = evaporation rate, h = characteristic length (in this case the film thickness), and D = diffusion coefficient. Sh is largest for the largest h i.e., for $h = h_{tr}$

References

- Acrivos, A., Shah, M., Petersen, E., 1960. On the flow of a non-newtonian liquid on a rotating disk. *J. Appl. Phys.* 31 (6), 963–968.
- Ay, F., Kocabas, A., Kocabas, C., Aydinli, A., Agan, S., 2004. Prism coupling technique investigation of elasto-optical properties of thin polymer films. *J. Appl. Phys.* 96 (12), 7147–7153.
- Baker, A., Dyer, P., 1993. Refractive-index modification of polymethylmethacrylate (pmma) thin films by krf-laser irradiation. *Appl. Phys. A* 57 (6), 543–544.
- Birdi, K., Vu, D., Winter, A., 1989. A study of the evaporation rates of small water drops placed on a solid surface. *J. Phys. Chem.* 93, 3702–3703.
- Bornside, D., Macosko, C., Scriven, L., 1989. Spin coating: one-dimensional model. *J. Appl. Phys.* 66 (11), 5185–5193.
- Bornside, D., Macosko, C., Scriven, L., 1991. Spin coating of a pmma/chlorobenzene solution. *J. Electrochem. Soc.* 138 (1), 317–320.
- Cochran, W., 1934. The flow due to a rotating disc. *Math. Proc. Cambridge Philos. Soc.*, vol. 30. Cambridge University Press, pp. 365–375.
- De Gennes, P.G., 2002. Solvent evaporation of spin cast films: crust effects. *Eur. Phys. J. E: Soft Matter Biol. Phys.* 7 (1), 31–34.
- Ebbens, S., Hodgkinson, R., Parnell, A.J., Dunbar, A., Martin, S.J., Topham, P.D., Clarke, N., Howse, J.R. In situ imaging and height reconstruction of phase separation processes in polymer blends during spin coating.
- Emslie, A.G., Bonner, F.T., Peck, L.G., 1958. Flow of a viscous liquid on a rotating disk. *J. Appl. Phys.* 29 (5), 858–862.
- Flacker, B.H., Soong, 1984. A mathematical model for spin coating of polymer resists. *J. Appl. Phys.* 56 (4), 1199–1206.
- Frank, C., Rao, V., Despotopoulou, M., Pease, R., et al., 1996. Structure in thin and ultrathin spin-cast polymer films. *Science* 273 (5277), 912.
- Guerrier, B., Bouchard, C., Allain, C., Benard, C., 1998. Drying kinetics of polymer films. *AIChE J.* 44 (4), 791–798.
- Haas, D.E., Quijada, J.N., Picone, S.J., Birnie, D.P., 2000. Effect of solvent evaporation rate on skin formation during spin coating of complex solutions. *Sol-Gel Opt. V* 3943, 280–284.
- Heriot, S.Y., Jones, R.A., 2005. An interfacial instability in a transient wetting layer leads to lateral phase separation in thin spin-cast polymer-blend films. *Nat. Mater.* 4 (10), 782–786.
- Hernandez, J., Rueda, D., Garcia-Gutierrez, M., Nogales, A., Ezquerro, T., Soccio, M., Lotti, N., Munari, A., 2010. Structure and morphology of thin films of linear aliphatic polyesters prepared by spin-coating. *Langmuir* 26 (13), 10731–10737.
- Jenekhe, S.A., 1984. Effects of solvent mass transfer on flow of polymer solutions on a flat rotating disk. *Indus. Eng. Chem. Fundam.* 23 (4), 425–432.
- Jukes, P.C., Heriot, S.Y., Sharp, J.S., Jones, R.A., 2005. Time-resolved light scattering studies of phase separation in thin film semiconducting polymer blends during spin-coating. *Macromolecules* 38 (6), 2030–2032.
- Karpitschka, S., Weber, C.M., Riegler, H., 2015. Spin casting of dilute solutions: vertical composition profile during hydrodynamic-evaporative film thinning. *Chem. Eng. Sci.* 129, 243–248.
- Köhler, R., Lazar, P., Riegler, H., 2006. Optical imaging of thin films with molecular depth resolution. *Appl. Phys. Lett.* 89 (24), 241906.
- Larson, R.G., Reh, T.J., 1997. *Spin Coating*. Springer, Netherlands, Dordrecht.
- Lawrence, C., 1988. The mechanics of spin coating of polymer films. *Phys. Fluids* (1958–1988) 31 (10), 2786–2795.
- Lawrence, C., 1990. Spin coating with slow evaporation. *Phys. Fluids A: Fluid Dynam.* (1989–1993) 2 (3), 453–456.
- Manske, L., Graves, D., Oldham, W., 1990. Dynamic measurements of film thickness over local topography in spin coating. *Appl. Phys. Lett.* 56 (23), 2348–2350.
- Mate, C.M., Novotny, V., 1991. Molecular conformation and disjoining pressure of polymeric liquid films. *J. Chem. Phys.* 94 (12), 8420–8427.
- Meyerhofer, D., 1978. Characteristics of resist films produced by spinning. *J. Appl. Phys.* 49 (7), 3993–3997.
- Mokarian-Tabari, P., Geoghegan, M., Howse, J., Heriot, S., Thompson, R., Jones, R., 2010. Quantitative evaluation of evaporation rate during spin-coating of polymer blend films: control of film structure through defined-atmosphere solvent-casting. *Eur. Phys. J. E* 33 (4), 283–289.
- Norrman, K., Ghanbari-Siahkali, A., Larsen, N., 2005. 6 studies of spin-coated polymer films. *Annu. Rep. Sect. C(Phys. Chem.)* 101, 174–201.
- Ohara, T., Matsumoto, Y., Ohashi, H., 1989. The film formation dynamics in spin coating. *Phys. Fluids A: Fluid Dynam.* (1989–1993) 1 (12), 1949–1959.
- Okazaki, M., Shioda, K., Masuda, K., Toei, R., 1974. Drying mechanism of coated film of polymer solution. *J. Chem. Eng. Jpn.* 7 (2), 99–105.
- Peurrung, L., Graves, D., 1991. Film thickness profiles over topography in spin coating. *J. Electrochem. Soc.* 138 (7), 2115–2124.
- Phillies, G.D., 1995. Hydrodynamic scaling of viscosity and viscoelasticity of polymer solutions, including chain architecture and solvent quality effects. *Macromolecules* 28 (24), 8198–8208.
- Picknett, R., Bexon, R., 1977. The evaporation of sessile or pendant drops in still air. *J. Colloid Interface Sci.* 61 (2), 336–350.
- Reisfeld, B., Bankoff, S., Davis, S., 1991a. The dynamics and stability of thin liquid films during spin coating. I. Films with constant rates of evaporation or absorption. *J. Appl. Phys.* 70 (10), 5258–5266.
- Reisfeld, B., Bankoff, S., Davis, S., 1991b. The dynamics and stability of thin liquid films during spin coating. II. Films with unit-order and large peclet numbers. *J. Appl. Phys.* 70 (10), 5267–5277.
- Shimoji, S., 1987. A new analytical model for spin coating process with solvent evaporation. *Japan. J. Appl. Phys.* 26 (6A), L905.
- Shimoji, S., 1989. Numerical analysis of the spin-coating process. *J. Appl. Phys.* 66 (6), 2712–2718.
- Soulie, V., Karpitschka, S., Flerence, L., Prene, P., Zemb, T., Moehwald, H., Riegler, H., 2015. The evaporation behavior of sessile droplets from aqueous saline solutions. *Phys. Chem. Chem. Phys.* 17, 22296–22303.
- Sukanek, P.C., 1991. Dependence of film thickness on speed in spin coating. *J. Electrochem. Soc.* 138 (6), 1712–1719.
- Toolan, D.T., Dunbar, A., Ebbens, S., Clarke, N., Topham, P.D., Howse, J.R., et al., 2013. Direct observation of morphological development during the spin-coating of polystyrene–poly (methyl methacrylate) polymer blends. *J. Polym. Sci., Part B: Polym. Phys.* 51 (11), 875–881.
- Washo, B., 1977. Rheology and modeling of the spin coating process. *IBM J. Res. Dev.* 21 (2), 190–198.
- Weill, A., Dechenaux, E., 1988. The spin-coating process mechanism related to polymer solution properties. *Polym. Eng. Sci.* 28 (15), 945–948.